PCCP

PAPER

View Article Online
View Journal | View Issue

Cite this: *Phys. Chem. Chem. Phys.*, 2014, **16**, 20157

Electronic stability and electron transport properties of atomic wires anchored on the MoS_2 monolayer†

Ashok Kumar,[ab] Douglas Banyai,[a] P. K. Ahluwalia,[b] Ravindra Pandey*[a] and Shashi P. Karna[c]

Received 15th May 2014,
Accepted 29th July 2014

DOI: 10.1039/c4cp02128b

www.rsc.org/pccp

The stability, electronic structure, and electron transport properties of metallic monoatomic wires anchored on the MoS_2 monolayer are investigated within the density functional theory. The anchoring of the atomic wires on the semiconducting monolayer significantly modifies its electronic properties; the metallic characteristics of the assembled monolayers appear in the density of states and band structure of the system. We find that Cu, Ag and Au wires induce the so-called n-type doping effect, whereas Pt wires induce a p-type doping effect in the monolayer. The distinctly different behavior of Pt–MoS_2 compared to the rest of the metallic wires is reflected in the calculated current–voltage characteristics of the assembled monolayers with a highly asymmetric behavior of the out-of-the-plane tunneling current with respect to the polarity of the external bias. The results of the present study are likely to extend the functionality of the MoS_2 monolayer as a candidate material for the novel applications in the areas of catalysis and optoelectronic devices.

1. Introduction

Two-dimensional molybdenum disulfide (MoS_2) has received considerable attention[1–8] since its synthesis has been carried out by the exfoliation technique[9] similar to the one applied to graphene. Under ambient conditions, the bulk MoS_2 has a hexagonal structure with the space group of $P63/mmc$,[10,11] in which a layer of Mo atoms is sandwiched between two layers of S atoms. This atomic trilayer configuration is referred as a monolayer.[11] The atoms within the MoS_2 monolayer are covalently bonded, whereas individual atomic sheets are bonded *via* weak van der Waals force. Although the bulk MoS_2 is a semiconductor with an indirect gap, the monolayer has a direct gap.[12–14] The monolayers of MoS_2 have versatile and tunable properties,[15–17] which are useful for their applications in nanoelectronics.[2,18] They also complement graphene in applications which require thin transparent semiconductors and are expected to have excellent gas sensing performance due to high surface-to-volume ratio.[19,20]

The fabrication of electronic devices for next-generation applications generally requires a combination of conducting and insulating materials, using which higher performance and greater flexibility can be achieved.[21–25] For example, Ag nanowires deposited on graphene led to significant enhancement in the conductivity of the functionalized graphene. Consequently, the Ag–graphene system has a greater potential in the high performance, flexible energy conversion and storage devices.[21] In addition, the incorporation of Au nanoparticles on MoS_2 by chemical and microwave routes resulted in a significant modulation of its electrical and thermal conductivity. The Au–MoS_2 device showed nearly a 9-fold increase in the effective gate capacitance, a low Schottky barrier ($\sim$14.5 meV) and an increase in its thermal conductivity ($\sim$23 W mK^{-1}).[22] Considering these experimental results, we are intrigued by the role played by the metallic nanostructures in modifying the electronic properties of a monolayer substrate. Does the effect solely come from nanostructures or does the interfacial chemistry of the nanostructure with monolayer play a dominant role? Specifically, we will focus on the monoatomic wires of Cu ($4s^1\ 3d^{10}$), Ag ($5s^1\ 4d^{10}$), Au ($6s^1\ 5d^{10}$) and Pt ($6s^1\ 5d^9$) anchored on the MoS_2 monolayer and on the calculation of their stability and electronic properties using the density function theory (DFT). Note that the metallic monoatomic wires, including Ag, Au and Pt, have been synthesized in the break-junction experiments and on the substrate.[26–29] The results of the present study are expected to extend the functionality of the MoS_2 monolayer as

[a] *Department of Physics, Michigan Technological University, Houghton, Michigan 49931, USA. E-mail: pandey@mtu.edu*
[b] *Department of Physics, Himachal Pradesh University, Shimla 171005, India*
[c] *US Army Research Laboratory, Weapons and Materials Research Directorate, ATTN: RDRL-WM, Aberdeen Proving Ground, MD 21005-5069, USA*

† Electronic supplementary information (ESI) available. See DOI: 10.1039/c4cp02128b

a candidate material for the novel applications in the areas of catalysis and optoelectronic devices.

2. Computational methods

Electronic structure calculations were performed within the generalized gradient approximation (GGA) with the Perdew–Burke–Ernzerhof (PBE) parameterization of the exchange and correlation functional form. The norm-conserving, relativistic pseudopotentials[30] as implemented in the SIESTA program package[31] were used in a fully separable non-local Kleinman and Bylander form to treat electron–ion interactions. The Kohn–Sham orbitals were expanded in a linear combination of numerical pseudoatomic orbitals using split-valance double-zeta with polarization (DZP) basis sets for all atoms. The MoS_2 monolayer, atomic wire and wire–monolayer systems were simulated in the *xy* plane using the supercell approximation and periodic boundary conditions. A vacuum distance of 15 Å along the *z*-direction was used to ensure negligible interactions between 2D system images. All calculated equilibrium configurations are fully relaxed, with residual forces smaller than 0.01 eV $Å^{-1}$.

3. Results and discussion

3.1 Structural properties

For the pristine MoS_2 monolayer, the calculated lattice constant is 3.23 Å, and the values for the Mo–S bond length and S–Mo–S bond angle are 2.47 Å and 82°, respectively. These GGA-PBE values are in complete agreement with the previously reported calculations on the pristine monolayer.[12–14] Note that the structural configuration of the MoS_2 monolayer shows the location of each Mo atom at the center of a trigonal prismatic cage formed by six S atoms.

The calculated lattice constants of the monoatomic linear wires of Cu, Ag, Au and Pt are 2.42, 2.65, 2.60 and 2.50 Å, respectively. Employing the projected augmented wave (PAW) method, the GGA-PBE values were previously reported as 2.33, 2.68, 2.61 and 2.35 Å for Cu, Ag, Au and Pt monoatomic wires, respectively.[32] A difference of about 6% in the value of the lattice constant of Pt may be due to the nature of pseudopotentials used in the PAW method because in our study, the norm-conserving, relativistic pseudopotentials were used to represent the core orbitals for Pt. Moreover, Pt is different from the other noble metal wires considered in terms of the valance electronic configuration, which may have different dependence of pseudopotential parameters in theoretical methods, such as the choice of cut-off radius, choice of semicore states and non-linear exchange correlation correction for the interaction of core–valence electrons.

Due to a lattice mismatch between the monolayer and monoatomic wires (Table 1), we need to minimize the strain at the interface by the suitable choice of a supercell simulating the assembled monolayer. Our choice of a (5×1) supercell of the atomic wire with the (4×4) supercell of the monolayer leads to a mismatch of about 6.3%, 2.5%, 0.6% and 3.3% for the co-periodic lattices of Cu–MoS_2, Ag–MoS_2, Au–MoS_2, and Pt–MoS_2, respectively. Here, we define the lattice mismatch as the difference in the calculated lattice parameters of the (5×1) atomic wire and (4×4) monolayer. Particularly, for Cu–MoS_2, we have also considered the (4×1) supercell of Cu wire along with the (3×3) supercell of monolayer, which yields the mismatch of 0.1% for the co-periodic lattice of the wire–monolayer system. In this way, the role of the interfacial strains in modifying the electronic properties of the assembled monolayer can be investigated [see supplementary section,[33] Fig. S1–S3 in the ESI†].

Table 1 The calculated (average) distance between wire and monolayer ($R_{wire\text{-}layer}$), and the binding energy (E_b) of the assembled monolayer

		E_b (eV per atom)	
System	$R_{wire\text{-}layer}$ (Å)	Hollow site	Top site
Cu–MoS_2	2.3	0.34	0.32
Ag–MoS_2	2.8	0.14	0.12
Au–MoS_2	2.8	0.15	0.13
Pt–MoS_2	2.1	0.34	0.51

The alignment of atomic wires deposited on the surface of the MoS_2 monolayer can be considered *via* either the top or hollow sites; the former refers to the case where the metal atoms are directly on top of the S atoms, and the latter refers to the case where the metal atoms are positioned between the two S atoms, thus directly above the underlying Mo atoms of the monolayer (Fig. 1).

The preferred binding site was determined by calculating the total energy of the assembled monolayer by varying separation between the wire and the monolayer for both the top and hollow sites. The binding energy of the assembled system is defined with respect to the constituent components as $E_b = (E_{MoS_2} + E_{wire}) - (E_{wire}/MoS_2)$. A positive value of E_b indicates the stability of the assembled system.

The calculated results are listed in Table 1, which shows that the difference in the E_b of the hollow and top sites for Cu, Ag and Au is small, although the hollow site is slightly preferred over the top site ($\Delta E \approx 0.02$ eV). On the other hand, Pt certainly prefers the top site of the MoS_2 monolayer. The predicted order of stability at the top site is Pt > Cu > Ag ≈ Au for the assembled monolayers. Interestingly, calculations performed at the GGA-PBE level of theory on the diatomic molecules evaluate the binding energy/per atom as 2.39, 2.15, 1.86, and 1.94 eV for PtS, CuS, AgS and AuS molecules, respectively. Therefore, the nature of bonding at the molecular level appears to persist for the wire–monolayer system.

3.2 Electronic structure

In order to gain further insight into the strength of the interaction between metallic atomic wire and the MoS_2 monolayer, we analyze the charge density difference profile [*i.e.* $\Delta\rho = \rho_{MoS_2+wire} - (\rho_{MoS_2} - \rho_{wire})$], as shown in Fig. 2. Here, the red region represents the charge accumulation, while the green region represents the charge depletion in the assembled monolayers. We find the MoS_2 monolayer to be polarized and the

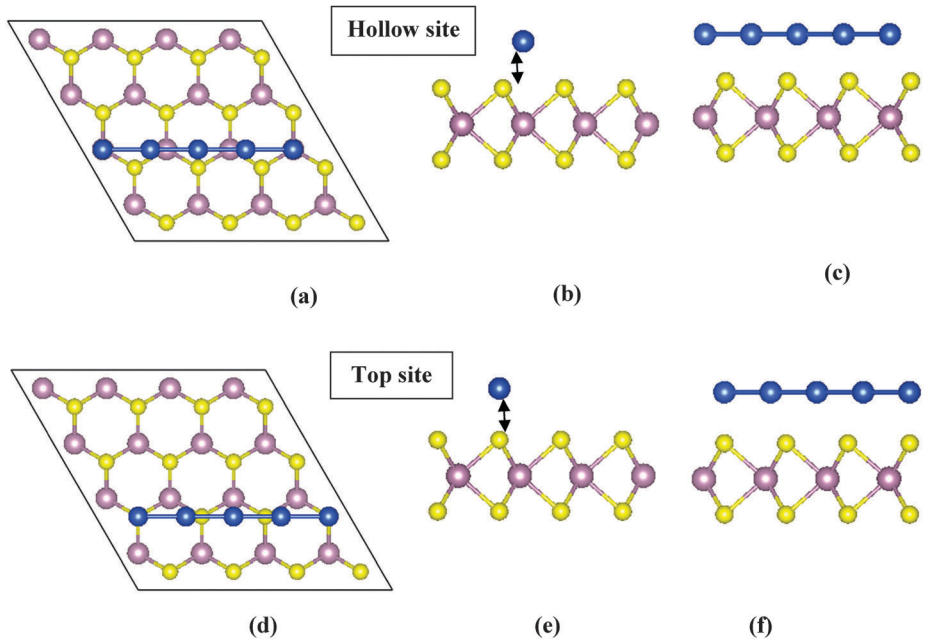

Fig. 1 (5 × 1) monoatomic wires on (4 × 4) MoS_2 monolayer: (a–c) top and side views of the hollow site; (d–f) top and side views of the top site. The brown, yellow, and blue circles represent Mo, S and atoms of the metallic wires, respectively.

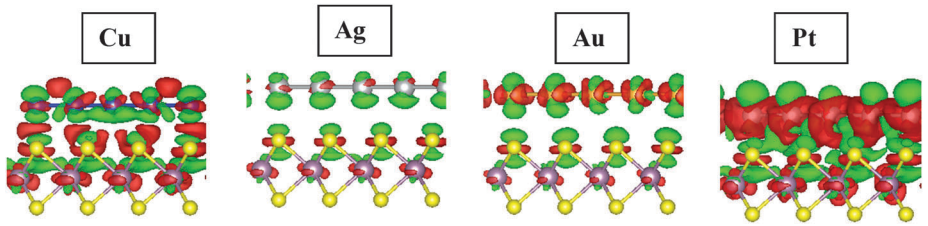

Fig. 2 A side view of the charge density difference contour plots. The red (green) regions correspond to the accumulation (depletion) regions of the charge density in the assembled monolayers. The isosurface value is taken as 0.001 e per $Å^3$.

induced polarization is relatively large for Pt–MoS_2 compared to the other assembled monolayers. This correlates well with the calculated equilibrium separations given in Table 1; the separation between the Pt wire and monolayer is much smaller than the corresponding separation in the other wire–monolayer systems. As shown in Fig. 2, the predicted order of stability (*i.e.* Pt > Cu > Ag ≈ Au) is assumed to be directly associated with the degree of polarization induced by wires in the assembled systems.

The analysis of Mulliken charges shows that all the monoatomic wires except Pt transfer a fractional charge of ∼0.05 e per atom to the monolayer, whereas Pt wire gains a fractional charge of ∼0.25 e from the monolayer. The partially occupied, spatially extended frontier orbitals of Pt appear to strongly interact with the monolayer following the fact that was predicted for the PtS molecule. The GGA-PBE calculations on diatomic molecules show that S gives a fractional charge to Pt in PtS, whereas Cu/Ag/Au transfer a fractional charge to S in other molecules. Note that the electronegativity difference between Mo (2.16) and S (2.58) atoms induces a fractional charge transfer of 0.3 e per atom from Mo to S atoms in the pristine monolayer. Thus, Cu, Ag and Au wires induce the so-called n-type doping effect, while Pt wire induces a p-type doping effect in the MoS_2 monolayer.

The electronic band structures of the assembled monolayers and pristine wires are displayed in Fig. 3. The interaction of the semiconducting MoS_2 monolayer with the metallic atomic wires significantly modifies its electronic properties. The metallic character of the assembled system appears in the projected density of states in which the metallic atoms of the atomic wires are associated with the electronic states near Fermi level (Fig. 4). Note that the metal wires are found to retain their bands in the assembled monolayers (Fig. 3). On the other hand, the pristine monolayer is semiconducting with a direct gap of 1.55 eV at point K (Fig. 3); the top of the valance band near Fermi energy is associated with mixed Mo-d and S-p states, whereas the bottom of the conduction band is mainly due to Mo-d states (see ESI,† Fig. S5[33]). This is not the case with the assembled monolayers where electronic bands at the Fermi level are partially occupied. A close examination of the valence band charge density of less than 0.5 eV below Fermi energy shows that the partially occupied bands are mainly associated with the atoms of the metallic wires. A small but noticeable contribution can also be seen from Mo

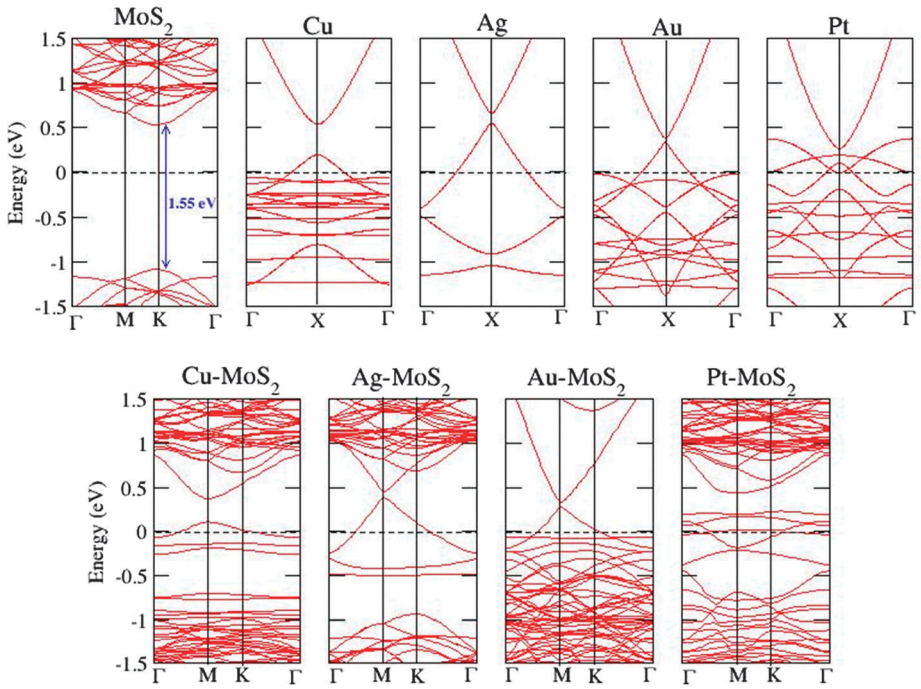

Fig. 3 Electronic band structures of (top panel) the pristine monolayer and wires and (down panel) the assembled MoS_2 monolayers.

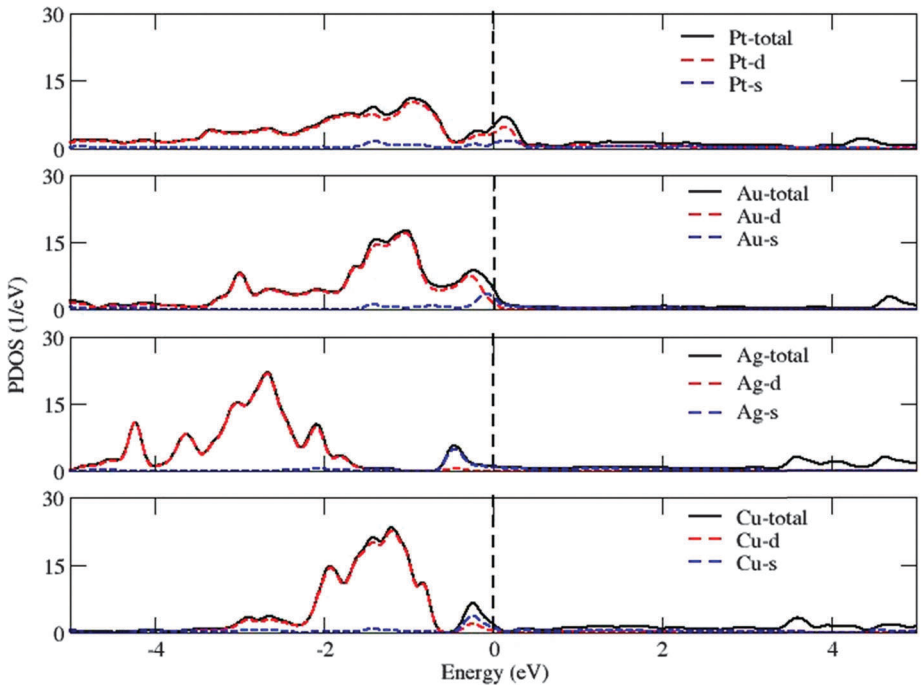

Fig. 4 Projected density of states of atomic wires for the assembled MoS_2 monolayers. Zero of the energy is aligned with Fermi energy.

and S atoms in the cases of Cu–MoS_2 and Au–MoS_2 for the states near Fermi level (Fig. 5), which are probably responsible for the different features of valence bands below Fermi energy of Cu–MoS_2- and Au–MoS_2-assembled monolayers compared with Ag–MoS_2 among the otherwise isoelectronic configured systems. Note that the appearance of overlapping spaghetti-like bands in the band structure is due to the choice of a large supercell simulating the assembled monolayers in the present study, which are due to strong hybridization between the Mo-d, S-p and metal wire-d orbitals, as can be seen in Fig. 4 and Fig. S5 (ESI†).

The frontier orbitals of Cu, Ag and Au are $s^1\ d^{10}$ and those of Pt are $s^1\ d^9$. This difference is reflected in Fig. 3 where the d-like localized electronic states form a flat band below Fermi level,

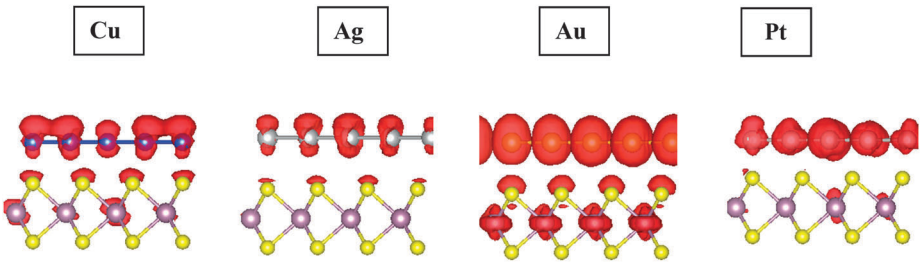

Fig. 5 A side view of the valance band charge density of the isosurface of 0.005 e $Å^{-3}$ below 0.5 eV Fermi level of the assembled monolayers.

and the s-like states for Cu–MoS_2, Ag–MoS_2, and Au–MoS_2 are represented by the bands crossing the Fermi level. On the other hand, the partially filled d-like band crosses the Fermi level for Pt–MoS_2. Thus, the conductivity of Pt–MoS_2 is likely to be dominated by the d-states of the Pt wire. Considering that the intrinsic quantum ballistic conductance of a given system can be estimated by the number of bands crossing the Fermi level, the ballistic conductance for Cu–MoS_2, Ag–MoS_2, Au–MoS_2 is estimated to be $2G_0$, whereas Pt–MoS_2 appears to have the estimated conductance of $4G_0$ (Fig. 3).

3.3 Electron transport properties

The metallic character is expected to appear in the enhanced conductance of the assembled monolayer rather than the conductance expected from the semiconducting pristine monolayer. In order to quantify this enhancement, we now calculate the current–voltage (*I–V*) characteristics of the assembled monolayers using a model setup employed in the scanning tunneling microscope (STM) measurements.[34] The tip is considered to be separated from the sample by a vacuum barrier width of 5 Å, mimicking a non-bonded tip configuration for the STM measurements. The cap configuration of the probe tip is modeled by a cage-like 43 atom Au cluster. The Bardin, Tersoff and Hamman (BTH) formulism[35,36] of electron tunneling was used to calculate the tunneling current in this model setup (see ESI,† Fig. S4[33]).

We define the bias to be positive when the sample is connected to a positive potential and electrons tunnel from the tip to the sample. It is notable that the tunneling current exponentially depends on the separation of the tip and the sample. Therefore, the choice of tip-sample separation will determine the magnitude of the tunneling current but should not affect the predicted trend for the considered assembled monolayers.

The calculated tunneling characteristics of the pristine and assembled monolayers are plotted in Fig. 6 for the bias range of −0.5 V to +0.5 V. Because the tunneling current is directly related to the convolution of DOS between the tip and sample, the appearance of finite DOS in the vicinity of the Fermi level of the wire–MoS_2 system is likely to be the reason of increase in tunneling current with the bias voltage, V_{bias}. The pristine MoS_2 monolayer is a semiconductor (Fig. 6), while the assembled monolayers show ohmic behavior for low forward bias of $\lesssim$0.3 V. For the reverse bias, asymmetric characteristics for the assembled monolayers appear with nearly constant current except Pt–MoS_2. Considering that the conduction channels

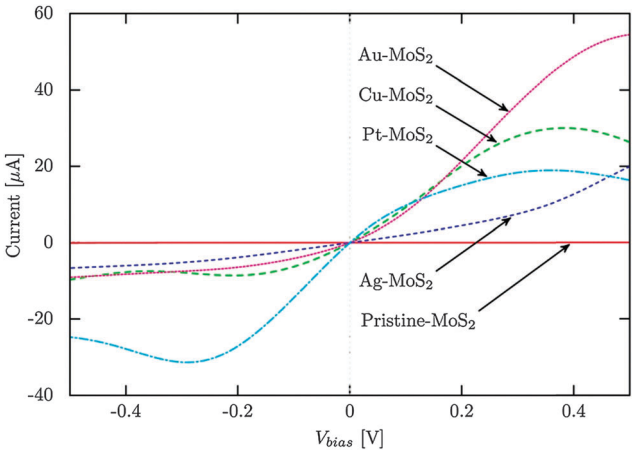

Fig. 6 The current–voltage (*I–V*) characteristics of the pristine and assembled monolayers.

under an applied bias are the states associated with atomic wires lined up near the Fermi level, the difference in the current–voltage characteristics (Fig. 6) can be understood in terms of the density of states of the assembled monolayers. For example, for the given bias, a relatively large tunneling current is seen for Au–MoS_2 compared to that for Ag–MoS_2. This difference can be attributed to the significantly large occupied states (states between 0 to −0.5 V in Fig. 3) for Au–MoS_2 (see ESI,† Fig. S5[33]). These states associated with atomic wires are lined up near the Fermi level and are the major tunneling "channels" under an applied bias. It is notable here that the appearance of unoccupied states near Fermi level in Pt–MoS_2 (Fig. 4, see ESI,† Fig. S5[33]) results in to a large tunneling current under the reverse bias (Fig. 6). Thus, the distinctly different behavior of Pt–MoS_2 compared with the rest of the metallic wire–MoS_2 monolayers may be attributed to the distinct nature of the bonding of Pt with the MoS_2 monolayer as previously discussed. It is notable here that electron transport across the MoS_2 monolayer coupled with Au and Ti contacts was theoretically investigated with the purpose of providing guidance for the choice of metallic contacts for MoS_2-based devices.[37]

4. Summary

In summary, the structural stability, electronic structure and electron transport properties of the metallic monoatomic wires

anchored on the MoS_2 monolayer are investigated. The calculated results show the stability of the assembled monolayers with Cu, Ag, Au and Pt wires. The electronic band structure and the density of states of the assembled monolayers reveal that states associated with metallic atomic wires appear in the vicinity of Fermi level, forming electron conduction channels. Cu–MoS_2, Ag–MoS_2, and Au–MoS_2 systems are found to possess $2G_0$ quantum ballistic conductance, while Pt–MoS_2 possesses $4G_0$ quantum conductance due to partially filled Pt-d states. The transverse current calculated for the assembled monolayers in the STM-like setup show significantly enhanced conduction relative to the MoS_2 pristine monolayer. Asymmetric current–voltage characteristics are predicted for the assembled monolayers except Pt–MoS_2, for which, a distinctly different nature of bonding is seen at the interface of the assembled monolayer. Our results unambiguously find the interaction of the MoS_2 monolayer with the metallic monoatomic wires to be relatively strong, modifying its electronic properties. Cu, Ag and Au wires induce an n-type doping effect, whereas Pt wire induces a p-type doping effect in the MoS_2 monolayer. The predicted interactions and doping effects of the monoatomic wires can be verified by various techniques, *e.g.* Raman spectra,[38] which can reflect changes in the electronic structure of the monolayer induced by metal wires. We believe that the results of the present study are likely to extend the functionality of the MoS_2 monolayer as a candidate material for the novel applications in the areas of catalysis and optoelectronic devices. It is well known that the catalytic activity is generally attributed to the unsaturated sites or excess charge on the surface of the nanomaterial. In the case of the MoS_2 monolayer, our results show that each of the S atoms have a charge of 0.3 e in excess, and the interaction of metal wires further induce n- or p-type doping effects in the pristine monolayer. Therefore, we believe that the interaction of metallic wires on MoS_2 is expected to enhance the catalytic activity, particularly in the hydrodesulfurization process.

Acknowledgements

Helpful discussions with Sanjeev K. Gupta, Xiaoliang Zhong, Mark Griep, Sankar Gowtham, Sandeep Nigam, Haiying He and Rodrigo Amorim are acknowledged. AK acknowledges the support of Michigan Technological University during his stay. RAMA and Superior, high performance computing clusters at Michigan Technological University were used in obtaining the results presented in this paper.

References

1 M. S. Xu, *et al.*, Graphene-Like Two-Dimensional Materials, *Chem. Rev.*, 2013, **113**(5), 3766–3798.
2 Q. H. Wang, *et al.*, Electronics and optoelectronics of two-dimensional transition metal dichalcogenides, *Nat. Nanotechnol.*, 2012, 7(11), 699–712.
3 S. Z. Butler, *et al.*, Progress, Challenges, and Opportunities in Two-Dimensional Materials Beyond Graphene, *ACS Nano*, 2013, 7(4), 2898–2926.
4 X. Huang, Z. Y. Zeng and H. Zhang, Metal dichalcogenide nanosheets: preparation, properties and applications, *Chem. Soc. Rev.*, 2013, **42**(5), 1934–1946.
5 X. F. Song, J. L. Hu and H. B. Zeng, Two-dimensional semiconductors: recent progress and future perspectives, *J. Mater. Chem. C*, 2013, **1**(17), 2952–2969.
6 A. Enyashin, S. Gemming and G. Seifert, Nanosized allotropes of molybdenum disulfide, *Eur. Phys. J.: Spec. Top.*, 2007, **149**, 103–125.
7 A. Kumar and P. K. Ahluwalia, *''Chapter 3: Tunable Electronic and Dielectric Properties of Molybdenum Disulfide'' under book title 'MoS$_2$: Materials, Physics, and Devices', MoS$_2$: Materials, Physics, and Devices,* Springer International Publishing, Switzerland, 2014, vol. 21, pp. 53–76.
8 P. P. Myskal Sagynbaeva, L. Yunguo and M. R. A. R. Ahuja, Tweaking the magnetism of MoS_2 nanoribbon with hydrogen and carbon passivation, *Nanotechnology*, 2014, **25**, 165703.
9 K. S. Novoselov, *et al.*, Two-dimensional atomic crystals, *Proc. Natl. Acad. Sci. U. S. A.*, 2005, **102**(30), 10451–10453.
10 J. Wilson and A. D. Yoffe, The transition metal dichalcogenides discussion and interpretation of the observed optical, electrical and structural properties, *Adv. Phys.*, 1969, **18**(73), 193–335.
11 A. Kumar and P. K. Ahluwalia, A first principle Comparative study of electronic and optical properties of 1H - MoS_2 and 2H - MoS_2, *Mater. Chem. Phys.*, 2012, **135**(2–3), 755–761.
12 K. F. Mak, *et al.*, Atomically Thin MoS_2: A New Direct-Gap Semiconductor, *Phys. Rev. Lett.*, 2010, **105**(13), 136805.
13 A. Splendiani, *et al.*, Emerging Photoluminescence in Monolayer MoS_2, *Nano Lett.*, 2010, **10**(4), 1271–1275.
14 A. Kumar and P. K. Ahluwalia, Electronic structure of transition metal dichalcogenides monolayers 1H-MX_2 (M = Mo, W; X = S, Se, Te) from ab-initio theory: new direct band gap semiconductors, *Eur. Phys. J. B*, 2012, **85**(6), 186.
15 A. Kumar and P. K. Ahluwalia, Tunable dielectric response of transition metals dichalcogenides MX_2 (M = Mo, W; X = S, Se, Te): Effect of quantum confinement, *Phys. B*, 2012, **407**(24), 4627–4634.
16 A. Kumar and P. K. Ahluwalia, Semiconductor to metal transition in bilayer transition metals dichalcogenides MX_2 (M = Mo, W; X = S, Se, Te), *Modell. Simul. Mater. Sci. Eng.*, 2013, **21**(6), 065015.
17 A. Kumar and P. K. Ahluwalia, Mechanical strain dependent electronic and dielectric properties of two-dimensional honeycomb structures of MoX_2 (X = S, Se, Te), *Phys. B*, 2013, **419**, 66–75.
18 B. Radisavljevic, *et al.*, Single-layer MoS_2 transistors, *Nat. Nanotechnol.*, 2011, **6**(3), 147–150.
19 H. Li, *et al.*, Fabrication of Single- and Multilayer MoS_2 Film-Based Field-Effect Transistors for Sensing NO at Room Temperature, *Small*, 2012, **8**(1), 63–67.
20 Q. Y. He, *et al.*, Fabrication of Flexible MoS_2 Thin-Film Transistor Arrays for Practical Gas-Sensing Applications, *Small*, 2012, **8**(19), 2994–2999.
21 J. Chen, *et al.*, Highly Conductive and Flexible Paper of 1D Silver-Nanowire-Doped Graphene, *ACS Appl. Mater. Interfaces*, 2013, **5**(4), 1408–1413.

22 T. S. Sreeprasad, *et al.*, Controlled, Defect-Guided, Metal-Nanoparticle Incorporation onto MoS_2 via Chemical and Microwave Routes: Electrical, Thermal, and Structural Properties, *Nano Lett.*, 2013, **12**(9), 4434–4441.
23 Y. Shi, J.-K. Huang, L. Jin, Y.-T. Hsu, S. F. Yu, L.-J. Li and H. Y. Yang, Selective Decoration of Au Nanoparticles on Monolayer MoS_2 Single Crystals, *Sci. Rep.*, 2013, **3**(5), 01839.
24 J. Huang, Z. Dong, Y. Li, J. Li, W. Tang, H. Yang, J. Wang, Y. Bao, J. Jin and R. Li, MoS_2 nanosheet functionalized with Cu nanoparticles and its application for glucose detection, *Mater. Res. Bull.*, 2013, **48**(11), 4544–4547.
25 J. Zhao, S. Yang, H. Zheng and Y. Li, Facile synthesis of MoS_2 nanosheet-silver nanoparticles composite for surface enhanced Raman scattering and electrochemical activity, *J. Alloys Compd.*, 2013, **559**(5), 87–91.
26 A. I. Yanson, *et al.*, Formation and manipulation of a metallic wire of single gold atoms, *Nature*, 1998, **395**(6704), 783–785.
27 B. H. Hong, *et al.*, Ultrathin single-crystalline silver nanowire arrays formed in an ambient solution phase. Science, *Science*, 2001, **294**(5541), 348–351.
28 N. Agrait, A. L. Yeyati and J. M. van Ruitenbeek, Quantum properties of atomic-sized conductors, *Phys. Rep.*, 2003, **377**(2–3), 81–279.
29 R. H. M. Smit, *et al.*, Common origin for surface reconstruction and the formation of chains of metal atoms, *Phys. Rev. Lett.*, 2001, **87**(26), 266102.
30 N. Troullier and J. L. Martins, Efficient Pseudopotentials for Plane-Wave Calculations. 2. Operators for Fast Iterative Diagonalization, *Phys. Rev. B: Condens. Matter Mater. Phys.*, 1991, **43**(11), 8861–8869.
31 J. M. Soler, *et al.*, The SIESTA method for ab initio order-N materials simulation, *J. Phys.: Condens. Matter*, 2002, **14**(11), 2745–2779.
32 E. Y. Zarechnaya, N. V. Skorodumova, S. I. Simak, B. Johansson and E. I. Isaev, Theoretical study of linear monoatomic nanowires, dimer and bulk of Cu, Ag, Au, Ni, Pd and Pt, *Comput. Mater. Sci.*, 2008, **43**, 522–530.
33 Provided as ESI†.
34 S. K. Gupta, *et al.*, Electron tunneling characteristics of a cubic quantum dot, $(PbS)_{32}$, *J. Chem. Phys.*, 2013, **139**, 244307.
35 J. Tersoff and D. R. Hamann, Theory and Application for the Scanning Tunneling Microscope, *Phys. Rev. Lett.*, 1983, **50**(25), 1998–2001.
36 J. Tersoff and D. R. Hamann, Theory of the Scanning Tunneling Microscope, *Phys. Rev. B: Condens. Matter Mater. Phys.*, 1985, **31**(2), 805–813.
37 Z. Bai, T. Markussen and K. S. Thygesen, arXiv:1311.2393v1, 11 Nov 2013.
38 B. G. Rao, H. S. S. R. Matte and C. N. R. Rao, Decoration of Few-Layer Graphene-Like MoS_2 and $MoSe_2$ by Noble Metal Nanoparticles, *J. Cluster Sci.*, 2012, **23**(3), 929–937.